Published in final edited form as:
Matrix Biol. 2014 February ; 34: 124–131. doi:10.1016/j.matbio.2013.10.006.

Heparin-dependent regulation of fibronectin matrix conformation

Brant Hubbard[1], **Jo Ann Buczek-Thomas**[2], **Matthew A. Nugent**[2,3,4,*], and **Michael L. Smith**[3,*]

[1]Molecular Biology, Cell Biology & Biochemistry Program, Boston University Boston, MA 02215

[2]Department of Biochemistry Boston University School of Medicine Boston, MA 02118

[3]Department of Biomedical Engineering, Boston University Boston, MA 02215

[4]Department of Biological Sciences University of Massachusetts Lowell Lowell, MA 01854

Abstract

Extracellular matrix (ECM) conformation is regulated by a variety of stimuli *in vivo*, including mechanical forces and allosteric binding partners, and these conformational changes contribute to the regulation of cell behavior. Heparin and heparan sulfate, for example, have been shown to regulate the sequestration and presentation of numerous growth factors, including vascular endothelial growth factor, on the heparin 2 binding domain in fibronectin (Fn). However, mechanical force also alters Fn conformation, indicating that the growth factor binding region may be co-regulated by both heparin and mechanical force. Herein, we describe a simple antibody-based method for evaluating the conformation of the heparin 2 binding domain in Fn, and use it to determine the relative contributions of heparin and mechanical strain to the regulation of Fn conformation. We achieved specificity in quantifying conformational changes in this region of Fn by measuring the ratio of two fluorescent monoclonal antibodies, one that is insensitive to Fn conformational changes and a second whose binding is reduced or enhanced by non-equilibrium conformational changes. Importantly, this technique is shown to work on Fn adsorbed on surfaces, single Fn fibers, and Fn matrix fibers in cell culture. Using our dual antibody approach, we show that heparin and mechanical strain co-regulate Fn conformation in matrix fibrils, which is the first demonstration of heparin-dependent regulation of Fn in its physiologically-relevant fibrillar state. Furthermore, the dual antibody approach utilizes commercially available antibodies and simple immunohistochemistry, thus making it accessible to a wide range of scientists interested in Fn mechanobiology.

Keywords

Fibronectin; extracellular matrix; heparin

[*]*Co-Corresponding authors:* Michael L. Smith Boston University 44 Cummington Mall ERB 502 Boston, MA 02215 Phone: 617-358-5489 msmith@bu.edu. Matthew A. Nugent University of Massachusetts Lowell 198 Riverside Street, Olsen 414A Lowell, MA 01854 978-934-2888 matthew_nugent@uml.edu.

Conflict of Interest Statement: The authors declare no competing financial interests.

1. Introduction

Cell function within multicellular organisms must be tightly coordinated to maintain homeostasis and to respond to changing demands placed on the organism. Consequently, cells constantly communicate with one another by releasing and receiving chemical, mechanical and electrical signals, and the ECM is one such medium used for transfer of information between cells (Vogel and Sheetz, 2006). This information is encoded in the chemical composition, molecular conformation, and supermolecular structure of the ECM. Whereas the chemical composition of the ECM in various tissues and organs has been defined through traditional biochemical methods, few tools are available to evaluate the conformational state of the ECM (Cao et al., 2012; Hertig et al., 2012; Smith et al., 2007). Furthermore, current approaches are insufficient to effectively evaluate the functional activity of the ECM as it relates to the conformational state of its components. These limitations are highlighted in studies that aim to understand the rapid responses of cells and tissues during development, wound repair and disease.

The ECM is principally comprised of proteins and polysaccharides, with the glycoprotein Fn being a prevalent component of the ECM during times of dynamic ECM remodeling such as wound healing, development, and the progression of diseases such as cancer and atherosclerosis (Hynes, 2009). The expression of Fn at these times and the large number of binding partners for Fn, including integrins and growth factors, make it a prime candidate for regulation of cell fate and signaling (Pankov and Yamada, 2002). Protein structure determines function, and both molecular Fn and Fn assembled into supermolecular fibers were demonstrated to have altered binding properties for ligands, and even altered bioactivity due to changes in their conformation (Little et al., 2009; Little et al., 2008; Mitsi et al., 2006; Zhong et al., 1998). A number of factors can influence Fn conformation, including denaturants, pH, mechanical forces, and allosteric binding partners (Alexander et al., 1979; Bradshaw and Smith, 2011; Khan et al., 1990; Mitsi et al., 2006). Multiple factors are presented simultaneously *in vivo*, although the combined influence of structure-altering factors are rarely considered in concert.

Heparan sulfate represents a family of structurally related linear polysaccharides that are found on cell surfaces and in the ECM throughout all animal tissues (Sarrazin et al., 2011). Heparin is a highly sulfated member of the heparan sulfate family that is found mainly in the storage granules of connective tissue mast cells (Sarrazin et al., 2011) and is released at cites of injury and inflammation where it has been shown to help the growth of embryonic stem cells (Furue et al., 2008). Heparan sulfates bind reversibly to Fn type III modules 12 to 14, thereby inducing a conformational change in Fn that is retained even after heparin unbinding (Mitsi et al., 2008; Mitsi et al., 2006). We have previously shown through ^{3}H-heparin binding assays that heparin is not retained by Fn after sample washing (Mitsi et al., 2006), which is consistent with the finding that heparin binding to Fn is relatively weak and destabilized under physiological ionic strength (Gold et al., 1983; Sekiguchi et al., 1983; Yamada et al., 1980). After heparin-dependent alteration of Fn conformation, the apparent affinity of Fn for growth factors, including vascular endothelial growth factor-A (VEGF), is dramatically increased as a consequence of increased availability of binding sites on Fn

(Martino and Hubbell, 2010; Mitsi et al., 2008; Mitsi et al., 2006; Smith et al., 2009). This interaction is specific for heparan sulfate, as chondroitin sulfate and desulfated derivatives of heparin do not increase VEGF binding (Mitsi et al., 2006).

Cell derived forces can mechanically strain Fn fibers (Smith et al., 2007), and the application of mechanical stress to Fn fibers leads to strain-induced alterations in the binding of numerous Fn ligands (Cao et al., 2012; Little et al., 2009; Little et al., 2008). These interactions can also alter cell attachment, as recent work has suggested that Fn binding sites for bacterial adhesins are disrupted with high levels of Fn fiber strain (Chabria et al., 2010), and alterations in the conformation of the 9^{th} and 10^{th} type III repeats can reduce cell attachment (Grant et al., 1997; Wan et al., 2013). The Fn molecule contains a large repertoire of binding sites for cell adhesion molecules, other ECM components, and cell signaling molecules (Hynes, 2009; Pankov and Yamada, 2002), and thus the role of mechanical forces in regulation of Fn competence for attachment of Fn binding partners has been of interest for some time.

In vivo, the ECM is exposed to both mechanical and chemical regulation of its conformation, and the combined effects are hypothesized to influence cell-signaling events. There is great interest in monitoring conformation changes of Fn, although currently available methods focus on mechanical strain-based conformation changes (Cao et al., 2012; Hertig et al., 2012). Antibodies (Abs) have been used for monitoring conformational changes of Fn for some time (Klein et al., 2003; Ugarova et al., 1995; Underwood et al., 1992; Zhong et al., 1998), however binding of an Ab cannot account for changes in Fn quantity. Here, we report on a dual Ab approach for monitoring heparin-mediated conformational changes in Fn within cell-generated Fn fibers in the ECM. A control Fn Ab with consistent binding affinity regardless of mechanical strain or heparin binding is used in conjunction with a conformation specific Ab. The ratiometric approach accounts for differences in Ab binding due to Fn quantity, thus overcoming limitations in previous approaches. Furthermore, this approach was used to determine the relative contribution of mechanical strain and heparin binding on the regulation of the activity of the growth factor-binding region of Fn in the 12th to 14th type III repeats of Fn. The Abs were initially screened using ELISAs, identifying heparin-sensitive Abs as well as a control Fn Ab that is conformation insensitive. The dual Ab technique was tested at the single fiber level and used to evaluate the mechanical impact on binding. Finally, the conformation of native cell made matrix was examined using the dual Ab screening system, demonstrating that this approach is competent for detection of heparin-dependent regulation of Fn conformation even in cell-derived ECM.

2. Results

Heparan sulfates are expressed by nearly every animal cell type and, as a pervasive component of the ECM, are regularly in contact with Fn, where they can induce conformational changes of Fn to promote the binding of growth factors such as VEGF (Martino and Hubbell, 2010; Mitsi et al., 2008; Mitsi et al., 2006). Detection of altered conformational states is a major technical challenge, especially *in vivo*, and thus we sought to identify Abs that are sensitive to heparin-induced conformational changes in Fn. We

chose to probe Abs that bind the Hep2, growth factor-binding domain of Fn, due to the importance of growth factor binding and presentation in regulation of cell behavior (Hudalla et al., 2011; Symes et al., 2010). Such Abs could then be used to detect heparin-mediated conformational changes in Fn matrix that render it competent for growth factor binding, even in complex cell culture and tissue environments, using widely accessible immunohistochemical approaches.

Quartz crystal microbalance with dissipation (QCMD) was chosen as a platform for examining the conformational regulation of heparin on surface absorbed Fn in real-time in aqueous conditions. For these experiments, Fn or bovine serum albumin (BSA) was adsorbed onto the chip surface causing a sharp reduction in frequency and increase in dissipation (Fig. 1). When the Fn-coated chip was exposed to phosphate buffered saline (PBS) alone or when the BSA coated chip was exposed to heparin for the remainder of the experiment, minimal changes in frequency or dissipation were observed. However when Fn-chips were exposed to heparin, a rapid increase in frequency and decrease in dissipation was observed (Fig. 1C, D). Both concentrations of heparin tested (10 μg/ml and 100 μg/ml) caused a similar maximal change in frequency and dissipation after prolonged exposure (Fig. 1C, D). However, the initial rates of change were greater for the higher heparin concentration. The differences in the rates of change are consistent with our previous work showing that heparin catalytically converts Fn from a globular to a stable elongated structure (Mitsi et al., 2008). The heparin-mediated change in Fn structure is also consistent with an overall reduction in the roughness of a fibronectin layer on a polystyrene surface (Mitsi et al., 2006), which would predict a loss of associated water (increased frequency) and a stiffer and more ordered surface (reduced dissipation). Moreover, the fact that heparin did not induce these changes on the BSA coated surface suggests that they are not an artifact of the addition of the highly charged heparin. Thus, QCMD provides additional evidence that heparin catalytically modifies Fn structure and offers a means to quantitatively monitor the kinetics of this process in real-time (Mitsi et al., 2006; Molino et al., 2012).

To determine if the heparin-induced conformational alteration in Fn might lead to altered Ab binding to the Hep2 region, we conducted a series of ELISAs on Fn treated with and without heparin using anti-Fn Abs specific for the Hep2 region and a control Ab raised to full-length Fn. Fn was adsorbed onto polystyrene plates and treated with heparin over a range of 0 to 100 μg/ml. After washing the plates to remove heparin (demonstrated in (Mitsi et al., 2006)), primary Abs were incubated with samples, followed by HRP-conjugated secondary Abs for analysis of binding with a spectrophotometer. Heparin treatment at the range of concentrations did not affect the binding of the control Fn Ab to the Fn-coated surfaces, confirmed by ANOVA (Fig. 2A). However, the binding of two Abs raised against the Hep2 domain was dependent upon whether Fn was pre-treated with heparin. A32 showed increased binding to heparin-pretreated Fn (Fig. 2B). Alternatively, MAB1935 showed decreased binding to Fn as the heparin concentration was increased (Fig. 2C). Thus, the heparin-induced conformational change in Fn appears to have altered the availability of the epitopes for these two Abs, with increased availability for A32 and reduced availability for MAB1935.

Cell contractile forces mechanically stretch Fn matrix fibers, and mechanical stress alters the molecular conformation of Fn within fibers (Bradshaw and Smith, 2011; Smith et al., 2007). Thus, we sought to determine whether mechanical tension applied to single fibers of Fn also altered the binding of monoclonal Ab A32. A32 was used since it demonstrated the largest relative change in binding to Fn in response to heparin treatment of Fn (i.e., 50% increase in binding; Fig. 2B). Single Fn fiber studies allowed for application of defined levels of strain to Fn fibers using previously described methods (Chabria et al., 2010; Little et al., 2009; Little et al., 2008). However, we improved our strain system by designing a novel device to produce a gradient in strain applied to Fn fibers, thus increasing the throughput of this approach. Fn fibers were stabilized by depositing them on stretchable sheets of polydimethylsiloxane (PDMS) (Fig. 3A, B). The strain gradient was established by making two incisions on a rectangular sheet of PDMS (Fig. 3A). Subsequent 1D application of strain leads to the largest degree of strain in the center of the PDMS sheet, which progressively diminishes when moving away from the center (Fig. 3B, C). In order to obtain local estimates of strain with this high throughput strain gradient device, a thin film of microfabricated ridges was applied on top of the PDMS sheet using previously described methods (Bradshaw and Smith, 2011; Klotzsch et al., 2009), and the distance between ridges was measured to allow strain to be calculated precisely at numerous points along the pattern. Fig. 3C demonstrates typical strain gradient values achievable with this device, although the overall range and magnitudes can be tuned by the extent of 1D strain application applied to the sheet.

Using this device, a three-color ratiometric approach was used to determine if Ab binding to Fn fibers was altered by mechanical strain or heparin treatment. First, artificial Fn fibers (Little et al., 2008) that were labeled with Alexa 546 fluorophores were deposited on top of the microfabricated ridges along the strain gradient (Fig. 3D, E). The use of fluorescently labeled Fn allowed an additional control for the amount of Fn in each pixel. Next, Fn fibers were either untreated, or treated with 50 μg/ml heparin. After rinsing the samples to remove heparin, the fibers were placed under various strain conditions. Fibers were then incubated with both the control Ab and A32, rinsed to remove primary antibodies, and incubated with corresponding fluorescently labeled secondary Abs for microscopic imaging (Fig. 3F, G). The relative binding of A32 was determined using an intensity ratio of secondary Ab bound to A32 Ab fluorescence divided by secondary Ab bound to control Fn Ab fluorescence. The control Fn Ab was shown to be strain independent by dividing its secondary Ab fluorescence by the intensity of fluorescently labeled Fn (data not shown). Intensity ratios were calculated for single fibers using areas of the fibers over valleys and not bound to ridges. Figure 3H shows the mean intensity ratios for single fibers of Fn over a range of strains with and without the addition of heparin. These data demonstrate that A32 binding was not affected by the mechanical strain state of Fn fibers in the absence of heparin. A32 binding was increased at all strain levels in heparin-pretreated versus the non-treated fibers, but there was a statistically significant decrease in A32 binding on fibers treated with heparin as fiber strain increased.

Next, we sought to determine whether our Ab-based system could be used to detect heparin-dependent conformational changes in cell made matrix. Bovine aortic endothelial cells (BAECs) were cultured in Labtech multi well chambers for four days to reach confluency

(Fig. 4A, B) and produce a robust Fn matrix. Following the culture period the cells were either untreated, or treated with 50 μg/ml heparin, washed, and fixed with paraformaldehyde. The state of the Fn matrix in untreated and heparin-treated samples was visualized with the control Ab (Fig. 4C, D, respectively) and A32 (Fig. 4E, F, respectively) after incubation with their respective fluorescently labeled secondary Abs. The relative binding of A32 was determined using a fluorescent intensity ratio of the secondary Ab bound to A32 divided by secondary Ab bound to the control Ab (Fig. 4G, H). The interconnected nature of cell-derived matrix is visible through immunohistochemical staining with both Abs and in untreated and heparin treated samples (Fig 4E, F, G, H), thus making single fiber analysis not feasible. Instead, approximately two million above-background pixels from 5 fields of view in 3 chambers were analyzed for both heparin treated and untreated matrix from multiple wells. Heparin treatment increased the intensity ratio of A32/Ctl, as indicated by the distribution of pixel intensities in the absence versus presence of heparin (Fig. 4I). Closer analysis of the intensity ratio distribution by reducing the number of intensity ratio bins shows that the conformation of only a subset of Fn matrix fibers was apparently altered by heparin treatment (Fig. 4J). The percentage of analyzed pixels at intensity ratios below 0.9 was similar for treated and untreated matrix, while the percentage of pixels with intensity ratios between 0.9 and 1.1 was markedly higher in untreated cells compared to heparin-treated samples. Conversely, heparin-treated samples had a much higher percentage of pixels with intensity ratios above 1.1 compared to untreated samples. The intensity ratio range for cell made matrix studies falls within the intensity ratio previously shown in Fig. 3H, quantitatively demonstrating that the cell made matrix provided an ensemble of fibers. The pixel analysis shown in Figure 4 is representative data that has been replicated in 3 experiments.

3. Discussion

Composition and conformation of the ECM influence cell behavior and fate. Whereas much is known about the composition of the ECM, there are few techniques available to probe the conformation of the ECM. Here we demonstrate that commercially-available Abs raised to the Hep2 domain of Fn showed alterations in binding to heparin-treated Fn adsorbed to polystyrene surfaces. This alteration in binding was also observed with Fn fibers, suggesting that these Abs could be used to detect conformational changes of Fn in biological ECM. Interestingly, the heparin induced increase in Ab binding was reduced, but not eliminated, as mechanical strain was applied to Fn fibers. Finally, we showed that the ratiometric method could be used to evaluate the conformational state of Fn within cell-derived ECM.

The structure of heparan sulfate, while not easily defined, is dynamic and shows interesting distinctions based on the tissue of origin, stage of development, and state of disease or injury (Shi and Zaia, 2009; Turnbull et al., 2001). Thus, it is possible that critical alterations in heparan sulfate structure that lead to changes in its ability to modulate Fn may play important roles in mediating cell function. In particular, the ability of heparan sulfate to mediate growth factor deposition within Fn-rich matrices may be used to localize growth factors for positional specific activity. Indeed, our previous work demonstrating that heparan sulfate is required for the platelet derived growth factor-mediated cell movements over Fn matrix that occur during gastrulation in the developing *Xenopus* embryo are likely reflective

of the ability of heparan sulfate to modify Fn conformation (Smith et al., 2009). Here, we provide a technique to image heparin-mediated changes in Fn. The ability to now probe the conformational state of biological matrices using the robust technique reported here will provide a means to explore the importance of this interesting process in a variety of settings. The dual Ab approach will also provide opportunities to examine other conformational changes as well by using other conformation specific Ab such as the mechanically sensitive L8 Ab (Little et al., 2009).

A number of techniques have been described to characterize non-equilibrium conformations of Fn. Two recently described methods for imaging Fn conformation are both dependent upon mechanical tension-induced conformational changes in Fn fibers and make use of phage-based molecular probes and peptides inspired by bacterial adhesins (Cao et al., 2012; Chabria et al., 2010). More complex probes for analyzing Fn conformation also exist and include Förster resonance energy transfer (Smith et al., 2007) and atomic force microscopy. Each of these techniques has been used with great success to explore various aspects of Fn conformation. Our technique builds on previous studies using mAbs to evaluate conformational changes in Fn (Klein et al., 2003; Ugarova et al., 1995; Zhong et al., 1998). However, our technique is distinct in that it uses a ratiometric approach where both antibodies are used simultaneously. Single probe tests cannot account for changes in the total amount of Fn, and thus a ratiometric approach with a control Ab that is conformation insensitive is needed to account for variations in the quantity of Fn. The use of commercially available monoclonal Abs that give precise information on the binding location on Fn using standard immunohistochemical approaches will allow this method to be easily implemented by a wide range of researchers. The technique requires minimal equipment and reagents besides the Ab and microscope for image acquisition. The technique provides consistent and comparable results for multiple experiments as demonstrated by the intensity ratios shown in Figure 3H and Figure 4I, J when all experimental and imaging parameters remain constant. Identification of other conformation specific Abs will provide additional application possibilities for the dual Ab conformation screening technique. Furthermore, enhanced dynamic range may be achieved by using a pair of Abs that both show conformation sensitivity (e.g., a ratio of A32 to MAB1935). Finally, a three color assay could also be employed whereby one control antibody is used with two additional antibodies that are sensitive to different regions or distinct conformational regulators.

Previous findings using atomic force microscopy showed an elongation of Fn molecules and decreased roughness of a monolayer of Fn after treatment with heparin (Mitsi et al., 2006). We have previously shown that the heparin-induced increase in binding of VEGF to full-length Fn is similar to the heparin-induced increase in binding of VEGF to the 40 kDa fragment of Fn that contains $III_{12\text{-}14}$ (Mitsi et al., 2008). This indicates that heparin causes a local change in III_{12}-14 that increases VEGF binding, although we cannot exclude that disruption of interactions between $III_{12\text{-}14}$ and other domains on the same molecule, or between molecules in the crowded environment of a Fn fiber also (Bradshaw et al., 2012) contributes to the increase in binding after heparin treatment. In the QCMD data shown in Fig. 1C and D, the addition of heparin to Fn adsorbed on the chip surface caused an increase in frequency and a decrease in dissipation, which indicates that heparin induced the Fn layer to become more rigid and organized. Based on these two findings it is logical that

mechanical strain could negate this effect by disrupting the Hep2 domain such that high levels of strain might partially or completely unfold the type III modules within III_{12} to III_{14}. The influence of mechanical force on heparin induced conformation may also explain the heterogenous binding profile of A32 to cell made matrix since it is known that Fn strain is not uniform. Cell made matrix staining showed an overall increase in the A32/control Ab ratio when treated with heparin. However, the distribution of pixel intensities suggests that a subset of Fn fibers are more sensitive to the heparin-induced effects. This result is supported by the finding that the heparin effect was reduced in single Fn fibers subjected to strain. Together these findings suggest that heparin and mechanical strain may co-regulate growth factor sequestration within Fn.

In vivo the ECM is exposed to numerous regulators at specific periods and in concert (Hynes, 2009). The ability to probe the conformation of Fn when exposed to multiple regulators will provide a critical step toward understanding how dynamic conformational changes influence cells and tissues. The dual Ab system presented here provides the versatility to explore the conformational impact of different regulators. The conformation-specific binding of A32 Ab shows that mechanical force and heparin co-regulate Fn structure. Expanding this technique to use other conformation specific Abs, such as L8 or ones yet to be determined, will provide the basis for exploring Fn conformation in a variety of physiological states. Future studies should explore the biological role of conformational regulation of Fn as it pertains to its ability to bind and modulate a number of growth factors (Martino and Hubbell, 2010; Mitsi et al., 2008; Wan et al., 2013).

4. Materials and Methods

4.1 Materials and Reagents

Fn was isolated from human serum using a previously published two-step chromatography process (Smith et al., 2007). Briefly, human serum (Valley Biomedical – Winchester, VA) was passed through a Sepharose 4B (Sigma – St. Louis, MO) column, and the eluent was then passed through a gelatin-Sepharose column (GE Healthcare – Barrington, IL). Fn was eluted from the column with 6M urea and verified with 280 nm absorbance on a NanoDrop 2000 spectrophotometer (Thermo Fisher Scientific Inc. – Billerica, MA).

Abs used in this study include A32 mouse anti-human Fn monoclonal Ab (Pierce – Rockford, IL – CSI 005-32-02) and MAB 1935 mouse anti-human Fn monoclonal Ab (Millipore – Billerica, MA – MAB1935), both of which bind to the Hep2 domain of Fn, rabbit anti-human Fn monoclonal Ab (Abcam – Cambridge, MA – ab32419) raised to full length human Fn, goat polyclonal secondary to mouse IgG conjugated with fluorescein (Jackson ImmunoResearch Laboratories Inc. – Westgrove, PA – 715-095-150), and goat polyclonal secondary to rabbit IgG conjugated to DyLight 650 (Abcam – ab96986). The Hep2 domain Abs, A32 and MAB1935, have previously been used to determine biological activity of Fn (Underwood et al., 1992; Underwood et al., 1993). A32 has previously been shown to specifically interact with $FnIII_{12\text{-}14}$ Underwood et al., 1992).

Heparin (heparin sodium porcine USP; 165 U/mg) was from porcine intestinal mucosa (Pharmacia HEPAR Inc. – Franklin, OH) and had an average molecular mass of 15 kDa.

4.2 Fn labeling

Fn was fluorescently labeled with Alexa 546 succinimidyl ester (Invitrogen – Grand Island, NY) on amines using previously published protocols (Smith et al., 2007). Fn was incubated with a 35-fold molar excess of Alexa 546 for 1 hour then the labeled Fn was separated from free dye by dialysis for 24 hours in PBS (Gibco – Grand Island, NY) (Cassette – Thermo – 10,000 MWCO). The solutions were characterized using a spectrophotometer to determine the Fn concentration and labeling ratio.

4.3 QCMD

Fn conformation studies were conduced on a Q-sense (Biolin Scientific – Linthicum Heights, MD) E4 QCMD. Standard quartz chips with gold electrodes were coated with a layer of polystyrene to maximize absorption of Fn. QCMD measures oscillation frequency and dissipation of a quartz crystal chip as an AC voltage is applied. The vibration frequency changes in response to the mass of material (i.e., Fn and associated water) adsorbed to the chip surface. The energy dissipation refers to the dampening of oscillation, where compact, rigid layers of adsorbed protein have lower dissipation values than soft and viscoelastic layers. We used the analysis of frequency and dissipation changes to obtain information regarding the conformational of an adsorped layer of Fn. An experimental temperature of 37° C was maintained by an attached heating unit for the QCMD. Frequency and dissipation values at several overtones were measured, and compared to accepted values, in air and liquid buffer (PBS) for each quartz chip prior to experiments to ensure proper functioning. A flow rate of 150 microliters per minute was used for all solutions during the experiments.

After appropriate baseline frequency and dissipation values were achieved in PBS (data not shown), Fn or BSA (Hyclone Laboratories – Billerica, MA) (0.1 mg/ml) was flowed over the chips for 10 minutes and then incubated for 15 min to achieve a stable layer of adsorbed protein on the chip surface. A small lag time is present between addition or protein or heparin and a corresponding change in frequency and dissipation. The chambers for the chips are approximately 600 μl in volume and there is a 6 inch length of tubing the solution must flow through before contacting the chip surface leading to a lag time. Chips were exposed to PBS until a stable frequency/dissipation signal was achieved and then PBS with and without heparin (10 or 100 μg/ml) was exposed to the chip surface under flow for 10 min. Flow was stopped and the chip was allowed to incubate with PBS (±heparin) for 30 min, and then flow was pulsed for an additional 10 min. This pulsing/incubation sequence was continued for the remainder of the experiment. Data was exported to Microsoft excel for analysis.

4.4 ELISAs

Fn (0.1 mg/ml; 100 μl/well) was adsorbed to the surface of 96 well polystyrene plates (Corning – Tewksbury, MA) at 4°C overnight. Fn solution was removed after 24 hours, and the plates were washed with tris buffered saline (TBS). Heparin solutions of increasing concentrations (0-100 μg/ml) were added to wells and incubated for one hour at room temperature. After incubation, the heparin solutions were removed, and the wells were washed three times with TBS (200 Ǝ1/well/wash). Primary Ab incubation was conducted after heparin treatment for one hour at room temperature with a dilution factor of 1:5,000 for

all primary Abs. The secondary Abs were HRP conjugated, and a KBL chromogenic system was used to quantify the relative amounts of Ab bound to Fn. Absorbance levels for each well were measured using a 96 well plate spectrophotometer (Optimax microtiter plate reader – Molecular Devices – Sunnyvale, CA).

4.5 Deposition of Fn fibers on strain device substrates

Artificial Fn fibers were deposited on the PDMS strain devices as previously described (Ejim et al., 1993; Little et al., 2008). PDMS sheets were placed in a custom 1-D strain device as previously described (Little et al., 2008; Smith et al., 2007). This device allowed deposited, labeled Fn fibers to be stretched or relaxed so that a range of strains could be tested for Ab binding. Briefly, a drop of Fn (1:10 mixture of unlabeled- and Alexa 546-Fn; final total concentration of 1 g/l) in PBS was placed on the PDMS sheet. A needle was used to draw the Fn from the surface of the drop and into a fiber that was deposited and attached to the substrate on contact. After deposition to the surface, the Fn fibers were carefully rinsed 3 times with water diameter from 1 to 3 μm. Fn fibers were then stretched or relaxed under water.

Some PDMS strain device surfaces were textured for analysis of local strain using a previously published technique (Bradshaw and Smith, 2011). Textured PDMS substrates with 20 μm tall ridges were prepared using soft lithography molding. A master mold was prepared by photolithography using su-8 20 resist (MicroChem Corp.- Newton, MA) on a silicon wafer. Polydimethylsiloxane (PDMS; Dow Corning Sylgard 184 – Wilmington, MA) was cast over the master mold to make a negative stamp of the desired 20 μm ridge features. This stamp was then made inert by plasma treatment (Harrick Plasma PDC-001 – Ithaca, NY) at 30W for 30 sec immediately followed by exposure to tetrafluorosilane vapor (Acros Organics - NJ) in a vacuum chamber for 30 min. This stamp was used to cast a drop of PDMS on top of a precast thin (.005″) PDMS sheet (Specialty Manufacturing Inc. – Saginaw, MI) with the ridge features used in the experiment. Next, the thin film of ridge features was treated in order to allow covalent attachment of Fn fibers as described (Klotzsch et al., 2009). Briefly, the substrate was exposed to plasma at 30W for 30 sec and then immediately exposed to aminosilane vapor (Acros Organics) in a vacuum chamber for 30 minutes. This was followed by covering the substrate in a 200 μl drop of 0.125% glutaraldehyde solution for 30 minutes then carefully washing with distilled water 3 times.

Strain gradients were created on single fibers of Fn by making incisions on a 6 cm (width) by 8 cm (length) rectangle of 0.005″ thick PDMS. Strain measurements were made at precise locations by measuring the valley width between micropatterned ridges on the PDMS pattern.

4.6 Cell culture/cell made matrix

BAECs were used for cell matrix studies. Cells were seeded onto eight well LAB-TEK II chamber slides (Nalge Nunc International – Naperville, IL) at a density of 25,000 cells/cm^2 and cultured for four days in Dulbecco's Modification of Eagle's Medium (Corning Cellgro – Mannassa, VA) containing 10% BSA and 1% pencillin-streptomycin solution (Corning Cellgro). Cells were treated with 200 μl/well of 50 μg/ml heparin solution for one hour at

room temperature. After heparin treatment cells were washed and fixed with 4% paraformaldehyde on ice for twenty minutes before analysis.

4.7 Immunohistochemistry

Immunohistochemistry was performed with both Abs (A32 and control Fn Ab) simultaneously with appropriate dilutions of primary and secondary Abs. Incubations were conducted for one hour at room temperature. Primary and secondary Abs were diluted in a 4% bovine serum albumin (Sigma) solution at dilution ratios of 1:200 and 1:400 respectively.

4.8 Imaging and Analysis

Imaging of labeled Fn and fluorescent secondary Abs for single fiber and cell made matrix studies was carried out on an Olympus IX81 inverted microscope. Fluorescent images for each relevant channel were collected using 20X (0.45 NA) and 40X (1.15 NA) objectives and a Nikon camera. MetaMorph v7.7.40 software (Molecular Devices) was used to acquire digital images.

Image processing was performed in MATLAB 7.10.0 (The MathWorks – Natick, MA). Images for fluorescent secondary Abs for A32 and control Fn Ab were used to calculate an intensity ratio (A32 fluorescent intensity/control Fn Ab fluorescent intensity) for each pixel of the acquired images using our previously published approach for ratiometric imaging (Smith et al., 2007). The ratiometric approach normalizes for differences in the quantity of Fn, intensity ratio differences can then be directly attributed to differences in conformation specific antibody binding. Statistical analysis of the data was conducted using Microsoft Excel 2010. Statistically significant differences between group means were determined via a fixed-effects ANOVA for P values <0.05 based on a null hypothesis that all data were sampled from a population with the same mean. In addition, the standard error of the slope, *SE*, was used to determine if the Abs intensity ratios (A32/Ctl) have a statistically meaningful linear relationship with Fn fiber strain based on a null hypothesis that the slope of the linear regression line relating intensity ratio to Fn fiber strain, *b*, is equal to 0. The test statistic (*t*-score) was calculated according to $t=b/SE$, and the P-value was determined from *t* using a t distribution calculator.

Acknowledgments

This study was funded by NSF CBET grant 1150467 (MLS), NIH grant HL088672 (MAN), grant M2012014 from the BrightFocus Foundation (MAN), and a Departmental grant from the Massachusetts Lions Eye Research Fund, Inc. (MAN).

References

Alexander SS Jr. Colonna G, Edelhoch H. The structure and stability of human plasma cold-insoluble globulin. The Journal of biological chemistry. 1979; 254:1501–1505. [PubMed: 762148]

Bradshaw MJ, Cheung MC, Ehrlich DJ, Smith ML. Using molecular mechanics to predict bulk material properties of fibronectin fibers. PLoS computational biology. 2012; 8:e1002845. [PubMed: 23300425]

Bradshaw MJ, Smith ML. Contribution of unfolding and intermolecular architecture to fibronectin fiber extensibility. Biophysical journal. 2011; 101:1740–1748. [PubMed: 21961600]

Cao L, Zeller MK, Fiore VF, Strane P, Bermudez H, Barker TH. Phage-based molecular probes that discriminate force-induced structural states of fibronectin in vivo. Proceedings of the National Academy of Sciences of the United States of America. 2012

Chabria M, Hertig S, Smith ML, Vogel V. Stretching fibronectin fibres disrupts binding of bacterial adhesins by physically destroying an epitope. Nat Commun 1. 2010; 135

Ejim OS, Blunn GW, Brown RA. Production of artificial-orientated mats and strands from plasma fibronectin: a morphological study. Biomaterials. 1993; 14:743–748. [PubMed: 8218723]

Furue MK, Na J, Jackson JP, Okamoto T, Jones M, Baker D, Hata R, Moore HD, Sato JD, Andrews PW. Heparin promotes the growth of human embryonic stem cells in a defined serum-free medium. Proc Natl Acad Sci U S A. 2008; 105:13409–13414. [PubMed: 18725626]

Gold LI, Frangione B, Pearlstein E. Biochemical and immunological characterization of three binding sites on human plasma fibronectin with different affinities for heparin. Biochemistry. 1983; 22:4113–4119. [PubMed: 6615820]

Grant RP, Spitzfaden C, Altroff H, Campbell ID, Mardon HJ. Structural requirements for biological activity of the ninth and tenth FIII domains of human fibronectin. The Journal of biological chemistry. 1997; 272:6159–6166. [PubMed: 9045628]

Hertig S, Chabria M, Vogel V. Engineering mechanosensitive multivalent receptor-ligand interactions: why the nanolinker regions of bacterial adhesins matter. Nano letters. 2012; 12:5162–5168. [PubMed: 22938173]

Hudalla GA, Kouris NA, Koepsel JT, Ogle BM, Murphy WL. Harnessing endogenous growth factor activity modulates stem cell behavior. Integr Biol (Camb). 2011; 3:832–842. [PubMed: 21720642]

Hynes RO. The Extracellular Matrix: Not Just Pretty Fibrils. Science. 2009; 326:1216–1219. [PubMed: 19965464]

Khan MY, Medow MS, Newman SA. Unfolding transitions of fibronectin and its domains. Stabilization and structural alteration of the N-terminal domain by heparin. Biochem J. 1990; 270:33–38. [PubMed: 2396990]

Klein RM, Zheng M, Ambesi A, Van De Water L, McKeown-Longo PJ. Stimulation of extracellular matrix remodeling by the first type III repeat in fibronectin. J Cell Sci. 2003; 116:4663–4674. [PubMed: 14576359]

Klotzsch E, Smith ML, Kubow KE, Muntwyler S, Little WC, Beyeler F, Gourdon D, Nelson BJ, Vogel V. Fibronectin forms the most extensible biological fibers displaying switchable force-exposed cryptic binding sites. Proceedings of the National Academy of Sciences of the United States of America. 2009; 106:18267–18272. [PubMed: 19826086]

Little WC, Schwartlander R, Smith ML, Gourdon D, Vogel V. Stretched extracellular matrix proteins turn fouling and are functionally rescued by the chaperones albumin and casein. Nano letters. 2009; 9:4158–4167. [PubMed: 19743815]

Little WC, Smith ML, Ebneter U, Vogel V. Assay to mechanically tune and optically probe fibrillar fibronectin conformations from fully relaxed to breakage. Matrix Biol. 2008; 27:451–461. [PubMed: 18417335]

Martino MM, Hubbell JA. The 12th-14th type III repeats of fibronectin function as a highly promiscuous growth factor-binding domain. FASEB J. 2010; 24:4711–4721. [PubMed: 20671107]

Mitsi M, Forsten-Williams K, Gopalakrishnan M, Nugent MA. A catalytic role of heparin within the extracellular matrix. J Biol Chem. 2008; 283:34796–34807. [PubMed: 18845539]

Mitsi M, Hong Z, Costello CE, Nugent MA. Heparin-mediated conformational changes in fibronectin expose vascular endothelial growth factor binding sites. Biochemistry. 2006; 45:10319–10328. [PubMed: 16922507]

Molino PJ, Higgins MJ, Innis PC, Kapsa RMI, Wallace GG. Fibronectin and Bovine Serum Albumin Adsorption and Conformational Dynamics on Inherently Conducting Polymers: A QCM-D Study. Langmuir. 2012; 28:8433–8445. [PubMed: 22551342]

Pankov R, Yamada KM. Fibronectin at a glance. Journal of cell science. 2002; 115:3861–3863. [PubMed: 12244123]

Sarrazin S, Lamanna WC, Esko JD. Heparan sulfate proteoglycans. Cold Spring Harb Perspect Biol. 2011; 3

Sekiguchi K, Hakomori S, Funahashi M, Matsumoto I, Seno N. Binding of fibronectin and its proteolytic fragments to glycosaminoglycans. Exposure of cryptic glycosaminoglycan-binding domains upon limited proteolysis. J Biol Chem. 1983; 258:14359–14365. [PubMed: 6643486]

Shi X, Zaia J. Organ-specific heparan sulfate structural phenotypes. J Biol Chem. 2009; 284:11806–11814. [PubMed: 19244235]

Smith EM, Mitsi M, Nugent MA, Symes K. PDGF-A interactions with fibronectin reveal a critical role for heparan sulfate in directed cell migration during Xenopus gastrulation. Proc Natl Acad Sci U S A. 2009; 106:21683–21688. [PubMed: 19966216]

Smith ML, Gourdon D, Little WC, Kubow KE, Eguiluz RA, Luna-Morris S, Vogel V. Force-Induced Unfolding of Fibronectin in the Extracellular Matrix of Living Cells. PLoS Biol. 2007; 5:e268. [PubMed: 17914904]

Symes K, Smith EM, Mitsi M, Nugent MA. Sweet cues: How heparan sulfate modification of fibronectin enables growth factor guided migration of embryonic cells. Cell Adh Migr. 2010; 4:507–510. [PubMed: 20562530]

Turnbull J, Powell A, Guimond S. Heparan sulfate: decoding a dynamic multifunctional cell regulator. Trends Cell Biol. 2001; 11:75–82. [PubMed: 11166215]

Ugarova TP, Zamarron C, Veklich Y, Bowditch RD, Ginsberg MH, Weisel JW, Plow EF. Conformational transitions in the cell binding domain of fibronectin. Biochemistry. 1995; 34:4457–4466. [PubMed: 7535564]

Underwood PA, Dalton BA, Steele JG, Bennett FA, Strike P. Anti-fibronectin antibodies that modify heparin binding and cell adhesion: evidence for a new cell binding site in the heparin binding region. J Cell Sci. 1992; 102(Pt 4):833–845. [PubMed: 1385458]

Underwood PA, Steele JG, Dalton BA. Effects of polystyrene surface chemistry on the biological activity of solid phase fibronectin and vitronectin, analysed with monoclonal antibodies. J Cell Sci. 1993; 104(Pt 3):793–803. [PubMed: 7686170]

Vogel V, Sheetz M. Local force and geometry sensing regulate cell functions. Nat Rev Mol Cell Biol. 2006; 7:265–275. [PubMed: 16607289]

Wan AM, Chandler EM, Madhavan M, Infanger DW, Ober CK, Gourdon D, Malliaras GG, Fischbach C. Fibronectin conformation regulates the proangiogenic capability of tumor-associated adipogenic stromal cells. Biochimica et biophysica acta. 2013

Yamada KM, Kennedy DW, Kimata K, Pratt RM. Characterization of fibronectin interactions with glycosaminoglycans and identification of active proteolytic fragments. J Biol Chem. 1980; 255:6055–6063. [PubMed: 6771264]

Zhong C, Chrzanowska-Wodnicka M, Brown J, Shaub A, Belkin AM, Burridge K. Rho-mediated contractility exposes a cryptic site in fibronectin and induces fibronectin matrix assembly. The Journal of cell biology. 1998; 141:539–551. [PubMed: 9548730]

Highlights

- Heparin and mechanical strain co-regulate fibronectin conformation in matrix fibrils.
- A widely accessible technique was developed to monitor fibronectin conformation.
- Fibronectin adsorbed to surfaces, in single fibers, and in matrix fibers were analyzed.
- A dual antibody fluorescent ratiometric method is used to evaluate Fn conformation.

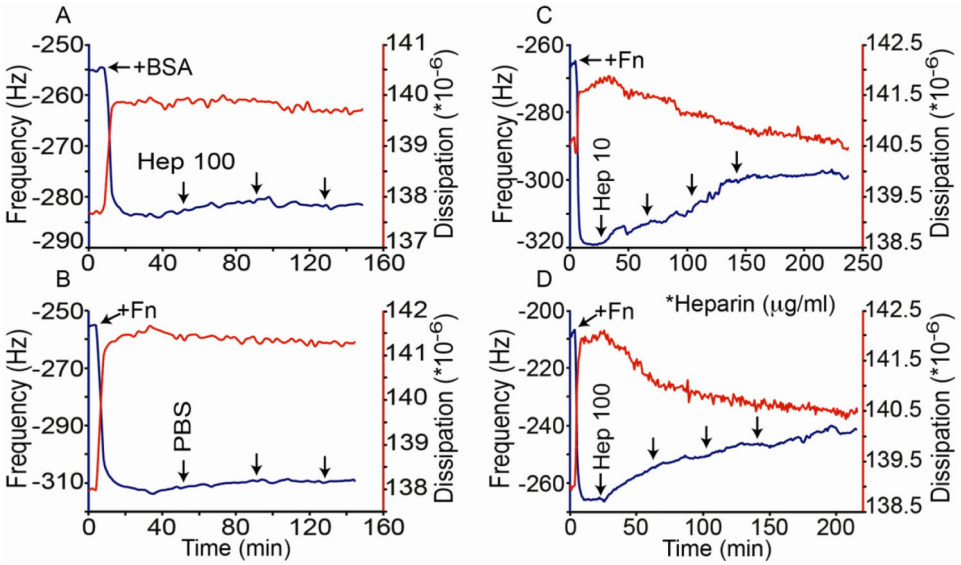

Figure 1.

Heparin-induced conformation changes shown by QCMD. A) Frequency (blue) and dissipation curves (red) are shown before and after adsorption of BSA to the chip which causes the initial decrease in frequency and increase in dissipation. Ten minute pulses of heparin (100 μg/ml) flowed over the chip surface followed by 30 minute incubations are indicated by the arrows. B) Frequency and dissipation curves are shown before and after adsorption of Fn to the chip. PBS was exposed to the chip surface using the same pulse flow/incubation sequence as described in A). C) and D) Frequency and dissipation data are shown after adsorption of Fn to the chip, followed by exposed to heparin at 10 or 100 μg/ml as indicated using the same pulse flow/incubation sequence as in panels A) and B). The addition of heparin to the Fn surfaces caused noticeable changes in frequency and dissipation. The observed initial rates of change of the frequency (F) and dissipation (D) were greater for the higher heparin dose ($\Delta F/\Delta T$ = 0.11 and 0.24 Hz/min; and $\Delta D/\Delta T$ = -1.3×10^4 and -2.1×10^4 units/min for 10 and 100 μg/ml heparin respectively). A similar heparin-induced change in frequency and dissipation of Fn coated chips was observed in 5 separate experiments.

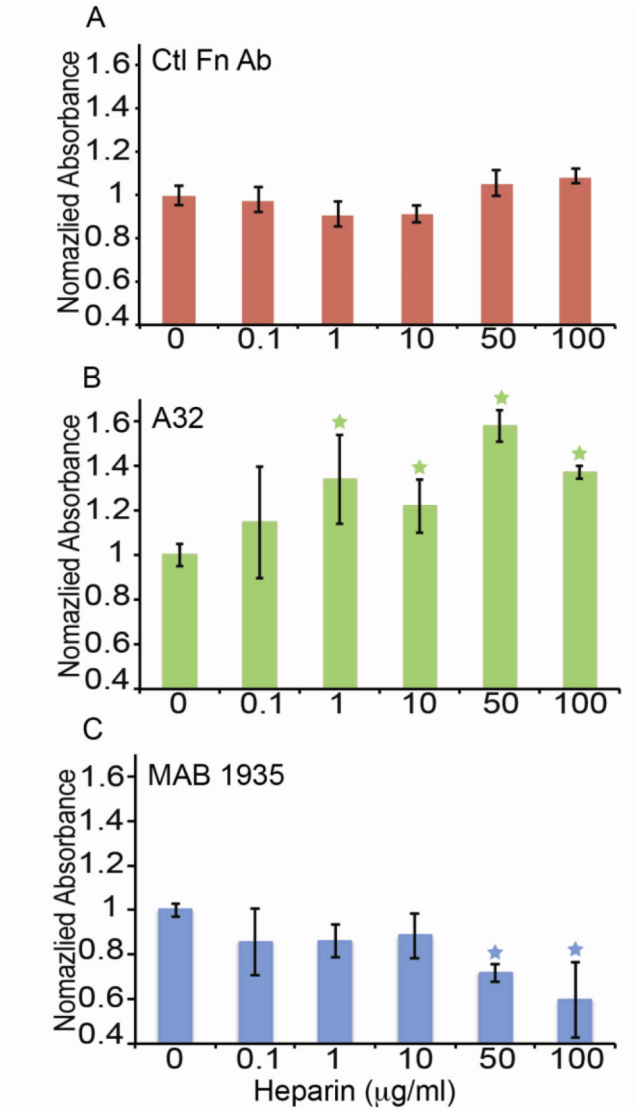

Figure 2.

ELISA data for the binding of Abs raised to the Hep2 domain (A32, MAB1935) and Ctl Fn Ab. A) Mean ± standard deviation ELISA values are shown for Ctl Fn Ab when exposed to a heparin concentration ladder (n=12) B) Mean ± standard deviation ELISA values for A32 are shown when exposed to the heparin concentration ladder and show an increase with heparin treatment (n=12). Values were normalized to the no heparin condition. C) Mean ± standard deviation ELISA values for MAB1935 are shown when exposed to the heparin concentration ladder and decrease with heparin treatment (n=12). Values were normalized to the no heparin condition. Asterisks indicate statistically significant trends according to ANOVA ($P<0.05$)

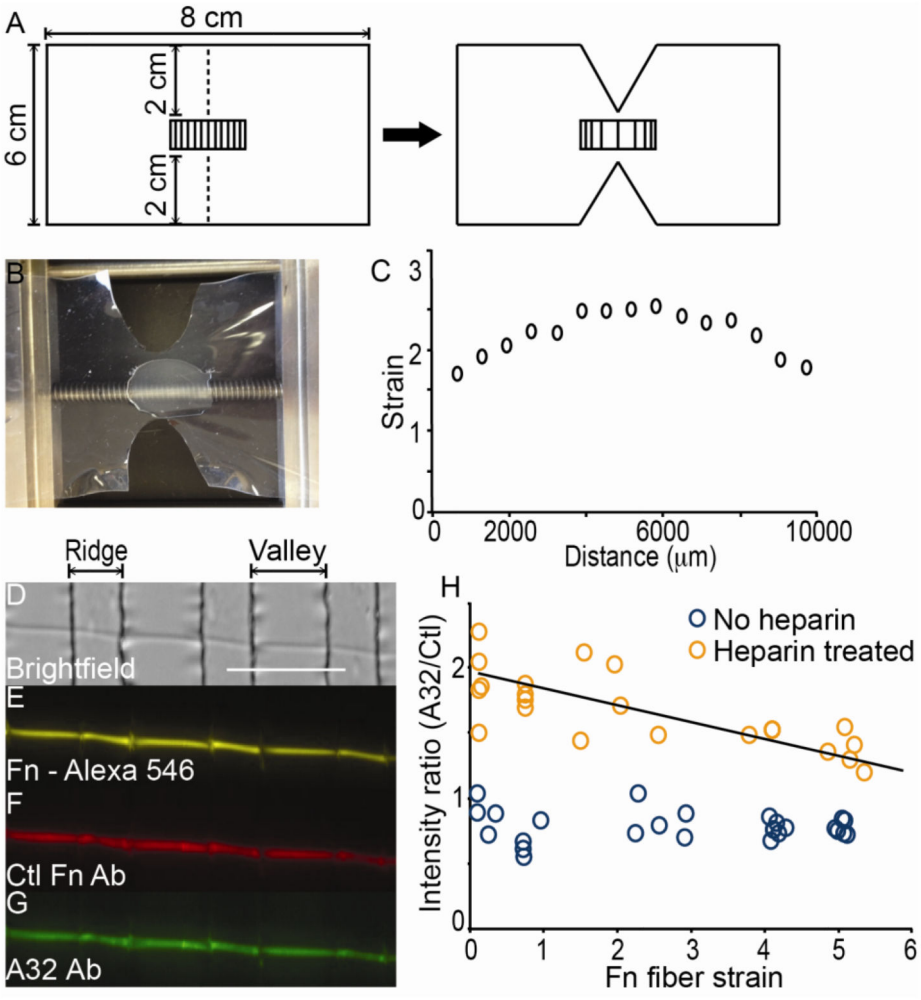

Figure 3.

Strain gradient creation and single Fn fiber staining with A32 and Ctl Fn Ab. A) A schematic for preparation of the strain gradient pattern is shown. The dimensions for a rectangle of PDMS, with micropatterned ridges, is shown with dotted lines indicating incision points. After application of strain to the sheet, the incision leads to a gradient with highest strain between the incision that decreases moving progressively away from the middle of the PDMS sheet. B) A representative image of a PDMS sheet with a strain gradient pattern is shown clamped within the strain device. The sheet is stretched to a length of 10.5 cm. C) The strain values were measured on a gradient-stretched PDMS substrate by measuring the width of microfabricated ridges/valleys, L_i. Relative strain was calculated according to L_i/L where L is the unstretched width of the valleys (20 μm). D-G) A brightfield image (D) is shown of a single Fn fiber fluorescently labeled with Alex-546 (E) after incubation with both the Ctl Fn Ab (F), the A32 Ab (G), and fluorescently labeled secondary Abs. H) Intensity ratios (A32/Ctl) are shown for Fn fibers stretched over a wide range of strains with (orange circles) or without prior exposure to heparin at 50 μg/ml (blue circles). Each circle represents one field of view for a single Fn fiber measured over the valleys. Four experiments for untreated and heparin treated fibers were conducted to

populate the graph. The regression of intensity ratio versus strain for heparin-treated fibers was statistically different from 0, showing a trend as a function of strain, by using the standard error of the slope. (scale bar = 100 μm). Line equation: $y = -0.1103x + 1.9177$.

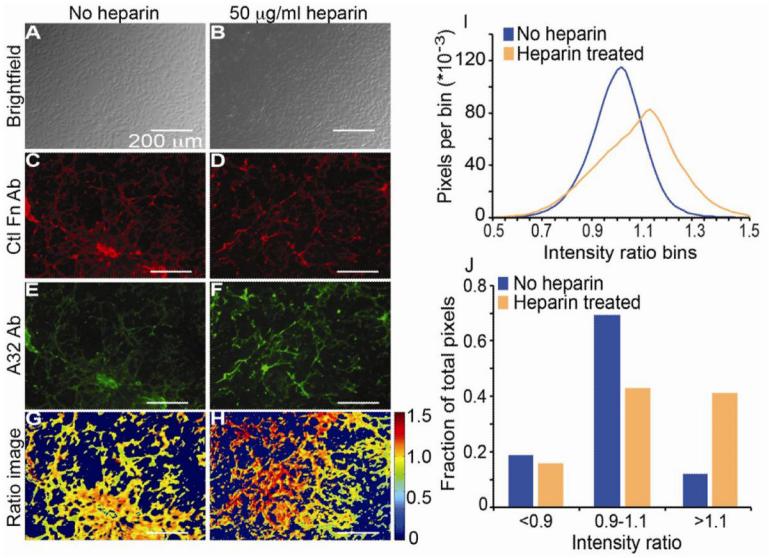

Figure 4.

BAEC-derived ECM staining with A32 and Ctl Fn Abs. A-B) Brightfield images of BAEC cultured to a confluent state and then untreated (A) or treated with 50 μg/ml heparin (B) are shown. C-D) Fluorescent microscopic images are shown of fixed BAEC samples without (C) or with heparin exposure (D) followed by incubation with Ctl Fn Ab and DyLight 650-labeled secondary. E-F) Fluorescent microscopic images are shown of fixed BAEC samples without (E) or with heparin exposure (F) followed by incubation with A32 Ab and FITC-labeled secondary. G-H) False-colored intensity ratio images are shown for BAEC samples without (G) and with heparin exposure (H). The colorbar indicates that range of ratios in the images. I) A histogram of intensity ratios is shown for all above background pixels from 5 fields of view from 3 samples with (orange line) or without heparin exposure (blue line). J) Histograms were broken into bins with values <0.9, between 0.9 and 1.1, and >1.1 so that the fraction of pixels in each bin is plotted with (orange) or without heparin exposure (blue). Pixel analysis of 5 images from 3 wells of cells.